Exceptional point magneto-optic isolators

ALEX J. GREDE, 1 NINA KRAINOVA, 1 AND NOEL C. GIEBINK 1,*

¹ Department of Electrical Engineering, The Pennsylvania State University, University Park, PA, 16802 * ncg2@psu.edu

Abstract: We show that operating magneto-optic coupled ring isolators near an exceptional point (EP) fundamentally improves their tradeoff between isolation bandwidth and insertion loss. In analogy to EP sensors, operating a coupled ring isolator at an EP causes its isolation bandwidth to depend on the square root of the nonreciprocal phase shift (NRPS) instead of the usual linear dependence, thereby enhancing the bandwidth when the NRPS is small. In cases of practical interest, this behavior enables more than a 50% increase in 20 dB isolation bandwidth at 3 dB insertion loss for a given pair of rings. The advantage of EP operation grows in the vicinity of magneto-optic material resonances and should extend to other types of on-chip isolators that rely on similarly-weak nonreciprocal perturbations.

© 2021 Optical Society of America under the terms of the OSA Open Access Publishing Agreement

1. Introduction

On-chip optical isolators and circulators are critical for the operation of many photonic integrated circuits, yet implementing these components on silicon with a foundry-compatible process that combines high isolation ratio and bandwidth with low insertion loss and physical footprint remains challenging. Of the various strategies [1–3] that have been explored to overcome this problem with full dynamic reciprocity [4], magneto-optic (MO) ring resonators [5–11] and Mach-Zender interferometers [12–15] are among the most successful to date. The nonreciprocal phase shift (NRPS) underlying the operation of these devices is, however, a weak perturbation (with a fractional change in propagation constant, $\Delta\beta/\beta \sim 10^{-4}$ between forward and backward-going modes), which imposes basic tradeoffs between isolation ratio, bandwidth, insertion loss, and compactness [1].

In parallel, recent work has demonstrated that the effect of a small perturbation, δ , can be greatly enhanced in non-Hermitian optical systems that operate near exceptional points (EPs), where the system eigenmodes and eigenfrequencies coalesce in parameter space [16–18]. These spectral degeneracies are characterized by eigenfrequencies that vary in proportion to $\sqrt[n]{\delta}$ (where n is the number of eigenmodes that coalesce) instead of the usual linear dependence on δ , which has garnered attention for sensing applications since the frequency shift measured in response to, e.g. a small dielectric perturbation remains large as the perturbation grows small [17, 18]. Viewing the weak NRPS of nonreciprocal MO devices in this context thus raises the question of whether operating near an EP could similarly improve their performance.

Here, we examine ring resonator-based MO isolators and circulators using temporal coupled mode theory [19, 20] and show that operating them near an EP leads to an analogous square root dependence of isolation bandwidth on NRPS that fundamentally improves its tradeoff with insertion loss. This result is verified through fullwave simulations and should be realizable in a previously fabricated coupled-ring circulator [21] simply by changing its mode of operation.

2. Results and discussion

2.1. Isolator behavior near an EP

We begin by considering a single ring isolator in the all-pass configuration shown in Fig. 1(a). Photons couple to and from the bus waveguide at a rate γ_a and are dissipated in the ring at a

rate γ_0 . Maintaining the same notation as Ref. [22] for consistency in what follows, the time evolution of the electric field in the ring, $E_0(t) = a_0(t)e^{-i\omega t}$, is described by:

$$\dot{E}_0(t) = -i\tilde{\omega}_0 E_0(t) + i\sqrt{\gamma_a/\tau_{\rm rt}} E_{\rm in}(t),\tag{1}$$

where $E_{\rm in} = a_{\rm in} e^{-i\omega t}$ is the incident field amplitude in the bus waveguide, $\tau_{\rm rt}$ is the round trip time in the ring, and $\tilde{\omega}_0 = \omega_0 - i\hat{\gamma}_0/2$ is its complex resonance frequency written in terms of the total loss rate, $\hat{\gamma}_0 = \gamma_{\rm a} + \gamma_0$. Defining the complex detuning, $\tilde{\delta}_0 = \omega - \tilde{\omega}_0$, Eq. 1 can be rewritten as $\dot{a}_0 = i\tilde{\delta}_0 a_0 + i\sqrt{\gamma_{\rm a}/\tau_{\rm rt}}a_{\rm in}$ which, together with the output boundary condition, $a_{\rm t} = a_{\rm in} + i\sqrt{\gamma_{\rm a}\tau_{\rm rt}}a_0$, yields the single ring transmission coefficient:

$$t_{\rm sr} = \frac{a_{\rm t}}{a_{\rm in}} = \frac{\delta_0 + i(\hat{\gamma}_0/2 - \gamma_{\rm a})}{\delta_0 + i\hat{\gamma}_0/2},\tag{2}$$

in terms of the real-valued detuning, $\delta_0 = \omega - \omega_0$. The intensity transmission coefficient, $T = |t_{\rm sr}|^2$, thus fully extinguishes at $\delta_0 = 0$ when $\gamma_a = \gamma_0$, which reflects the usual critical coupling condition where the loaded Q-factor of the ring is half its intrinsic Q-factor [23].

Due to the NRPS in the ring, the resonance frequency for forward-going (counter clockwise-circulating) light differs from that of backward-going (clockwise-circulating) light by an amount, δ_{mo} . Thus, if the ring in Fig. 1(a,i) is critically coupled and tuned to extinguish backward-going light at $\delta_0 = 0$, forward-going light is detuned (i.e. $\delta_0 \to \delta_0 - \delta_{\text{mo}}$), causing the transmission minimum of the black curve in Fig. 1(b) to shift to the right. An approximate analytical expression for the isolation bandwidth (defined as the frequency range over which a minimum inverse isolation ratio, $Y = T_{\text{B}}/T_{\text{F}} \ll 1$, is maintained) in this situation follows from Eq. 2:

$$b_{\rm sr} \approx \frac{2\gamma_0 \delta_{\rm mo} \sqrt{Y}}{(\delta_{\rm mo}^2 + \gamma_0^2)^{1/2}},\tag{3}$$

and exhibits a linear dependence on $\delta_{\rm mo}$ when $\delta_{\rm mo} \ll \gamma_0$. Given that the forward transmittance of the isolator at $\delta_0 = 0$ is $T_{\rm F} = \delta_{\rm mo}^2/(\delta_{\rm mo}^2 + \gamma_0^2)$, Eq. 3 can be rewritten as $b_{\rm sr} \approx 2\delta_{\rm mo}\sqrt{Y(1-T_{\rm F})}$, which expresses the basic tradeoff between bandwidth, isolation ratio, and insertion loss for a single ring isolator.

Now consider the situation depicted in Fig. 1(a,ii), where the original MO ring is coupled to the bus waveguide via another, non-MO ring. In analogy to the treatment above, the coupled mode equations that describe this system are:

$$\dot{a}_1 = i(\omega - \tilde{\omega}_1)a_1 + i\frac{\tilde{\kappa}}{2}a_2 + i\sqrt{\frac{\gamma_a}{\tau_{rt}}}a_{in}$$
(4a)

$$\dot{a}_2 = i(\omega - \tilde{\omega}_2)a_2 + i\frac{\tilde{\kappa}^*}{2}a_1. \tag{4b}$$

Assuming lossless coupling between the rings (i.e. $\tilde{\kappa} = \tilde{\kappa}^* = \kappa$) and maintaining the same complex detuning notation as before, $\tilde{\delta}_{1,2} = \omega - \tilde{\omega}_{1,2} = \delta_{1,2} + i\hat{\gamma}_{1,2}/2$, the transmission coefficient for this coupled ring case is [22]:

$$t_{\rm cr} = \frac{(\kappa/2)^2 - \tilde{\delta}_1 \tilde{\delta}_2 + i \gamma_a \tilde{\delta}_2}{(\kappa/2)^2 - \tilde{\delta}_1 \tilde{\delta}_2}.$$
 (5)

The eigenfrequencies of the homogeneous system in Eq. 4 follow from the poles of Eq. 5 and feature an EP when $|\hat{\gamma}_1 - \hat{\gamma}_2| = 2\kappa$. However, as emphasized by Smith *et al.* [22], the transmittance minima (assuming passive rings with no gain) that follow from Eq. 5 do not coincide with the eigenfrequencies due to interference with the input field in the bus waveguide.

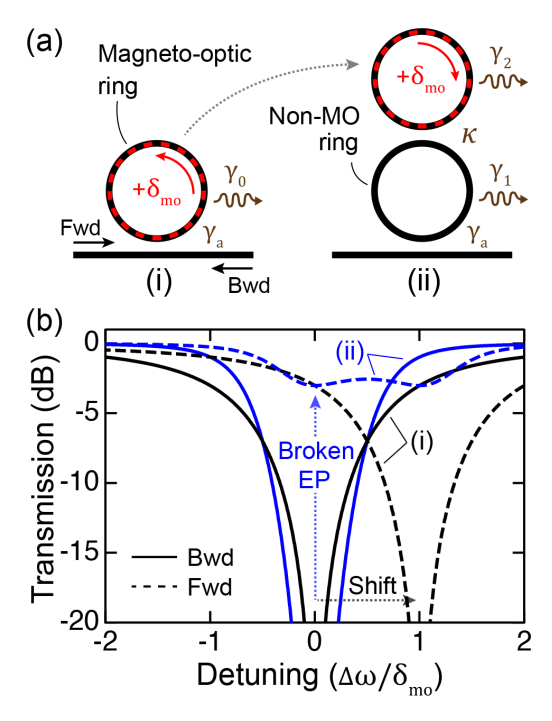


Fig. 1. (a) Schematic showing the single (i) and coupled (ii) ring isolator configurations; red dashes denote a magneto-optic ring with a resonance frequency split, δ_{mo} , between clockwise and counterclockwise circulating modes; the red arrow indicates the direction with the higher frequency. Photons are coupled to and from the bus waveguide at a rate, γ_a , and between the rings at rate κ . Squiggly arrows denote the photon dissipation rate in each ring. (b) Forward and backward transmission spectra for the critically-coupled single ring (black), where δ_{mo} simply shifts the resonance, and the coupled ring system (blue), where δ_{mo} breaks the exceptional point that exists for backward-going light.

The EP analogue in this case is the point at which a single transmittance minimum splits into two, and may be identified by setting the derivative of the transmittance, $dT(\omega)/d\omega = 0$. Recapping the result from Ref. [22], the splitting point (casually referred to as the EP hereafter) occurs when $\alpha \hat{\kappa}^4 + \beta \hat{\kappa}^2 + \chi = 0$, where $\hat{\kappa}^2 = (\hat{\gamma}_1 \hat{\gamma}_2 + \kappa^2)/4$, $\alpha = 2(\gamma_1 + 2\hat{\gamma}_2)$, $\beta = -\hat{\gamma}_2(\gamma_a \hat{\gamma}_2 + 2\gamma_{avg}^2)$, $\chi = \gamma_a \hat{\gamma}_2^2 \gamma_{avg}^2/2$, and $\gamma_{avg} = (\hat{\gamma}_1 + \hat{\gamma}_2)/2$.

To make a good isolator, the EP should ideally coincide with the critical coupling condition that fully extinguishes transmission in one direction [23]. This condition is found from the zeros of Eq. 5 and can be expressed as $\hat{\gamma}_2(\gamma_a - \gamma_1) = \kappa^2$. Combining this constraint with the splitting point criterion, it is then straightforward to show that both are satisfied when $\gamma_a - \gamma_1 = \hat{\gamma}_2 = \kappa$.

Implementing this condition with γ_1 set to zero for simplicity (i.e. negligible loss in the non-MO ring) thus yields a critically-coupled EP isolator characterized by the blue set of curves in Fig. 1(b). The backward transmission spectrum occurs when there is no detuning between the rings (i.e. δ_1 for CW circulation equals δ_2 for CCW circulation) and exhibits a sharper minimum than the single ring case since it is a second order filter [24]. In the case of forward-going light, the top ring is detuned by the MO frequency split ($\delta_2 \rightarrow \delta_2 - \delta_{mo}$), which breaks the EP and leads to the appearance of two shallow minima.

Setting aside the increase in isolation bandwidth that stems from its second order filter response, the most interesting feature of the EP isolator is that its isolation bandwidth scales as the *square* root of δ_{mo} rather than linearly as shown in Fig. 2(a). A fairer comparison to two cascaded single

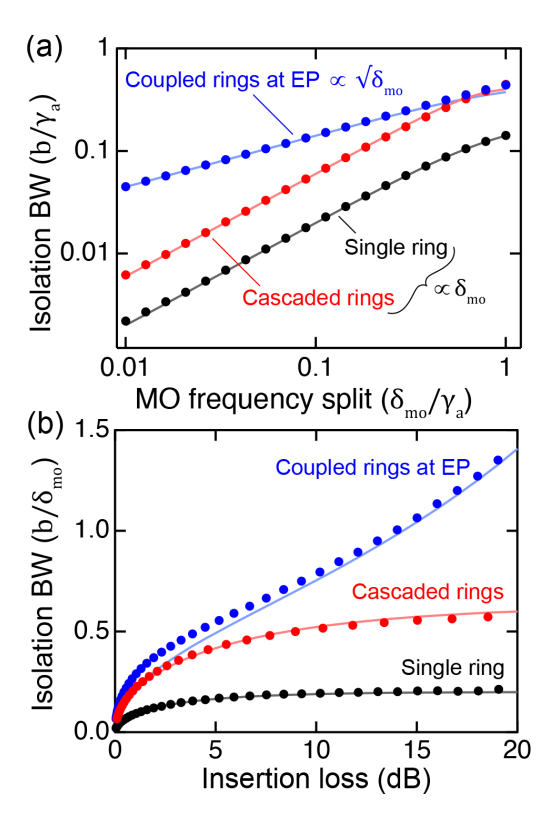


Fig. 2. (a) 20 dB isolation bandwidth as a function of the resonance frequency split in the MO ring from Fig. 1, normalized to its dissipation rate (equal to γ_a by virtue of critical coupling) for the case of a single ring isolator (black), two single ring isolators cascaded in series (red), and the coupled ring isolator operating at its exceptional point (blue). (b) Isolation bandwidth per unit MO frequency shift as a function of insertion loss for each case. The symbols in each panel are calculated by numerically evaluating the transmittance spectra and the solid lines reflect the analytical approximations given in the text.

ring isolators [11] with the same net footprint and filter order shows that the bandwidth advantage of EP operation emerges when δ_{mo} is small compared with the loss/coupling rates in the system ($\gamma_a = \gamma_2 = \kappa$ at the EP), similar to the enhancement regime for EP sensors [17, 18]. We note, however, that whereas some coupled ring EP sensors can actually perform better when operated away from their EP with $\kappa < \kappa_{ep}$ [25], operating at the EP is required in the present case for the isolation bandwidth to achieve the square root scaling shown in Fig. 2(a).

As in the single ring case, it is possible to derive an approximate analytical expression for the isolation bandwidth at the EP:

$$b_{\rm ep} \approx \frac{\sqrt{2\delta_{\rm mo}}\gamma_2 Y^{1/4}}{(\delta_{\rm mo}^2 + \gamma_2^2)^{1/4}},$$
 (6)

which explicitly shows the $\sqrt{\delta_{\rm mo}}$ dependence and agrees well with the numerical results in Fig. 2. Using the forward transmission at zero detuning (which is identical to the single ring isolator), Eq. 6 can be re-expressed in terms of the single ring isolator bandwidth as $b_{\rm ep} = b_{\rm sr} (4 Y T_{\rm F})^{-1/4}$, which indicates that the bandwidth enhancement grows arbitrarily large with increasing insertion loss. Figure 2(b) compares the bandwidth-insertion loss tradeoff for all three systems, demonstrating that EP operation enables a given MO frequency split to be used more efficiently.

2.2. Circulator behavior near an EP

Since the total loss in the upper ring of the EP isolator does not distinguish between dissipation and outcoupling, the results above are easily extended to the coupled ring circulator shown in Fig. 3(a) by setting $\hat{\gamma}_2 = \gamma_2 + \gamma_b$. The scattering matrix coefficient for the thru path (S_{21}) in this case is the same as Eq. 5 and that for the cross path (S_{31}) is obtained from the boundary condition for the output field at port 3, $a_x = i\sqrt{\gamma_b\tau_{rt}}a_2$, yielding:

$$S_{21} = \frac{(\kappa/2)^2 - \tilde{\delta}_1 \tilde{\delta}_2 + i \tilde{\delta}_2 \gamma_a}{(\kappa/2)^2 - \tilde{\delta}_1 \tilde{\delta}_2}$$
 (7a)

$$S_{31} = \frac{-i(\kappa/2)\sqrt{\gamma_a\gamma_b}}{(\kappa/2)^2 - \tilde{\delta}_1\tilde{\delta}_2}.$$
 (7b)

The intuitive mode of operation for this device is to employ co-directional MO frequency shifts in each ring that reinforce one another. This means that the rings have identical resonance frequencies in the absence of a magnetic field and, e.g. the CCW mode in the lower ring and CW mode in the upper ring undergo the same MO frequency shift (i.e. $\tilde{\delta}_{1,2} \to \tilde{\delta}_{1,2} - \delta_{\text{mo}}$) so that the extrema of $|S_{12}|^2$ and $|S_{13}|^2$ simply translate to the right in Fig. 3(b) and 3(c). This 'shift' mode of operation was analyzed previously in Refs. [10] and [11], and was experimentally demonstrated in Ref. [21]. The isolation bandwidth between ports 1 and 2 for critically coupled operation is:

$$b_{21,\text{shft}} \approx \frac{2\delta_{\text{mo}}\gamma_{\text{a}}Y^{1/4}}{(4\delta_{\text{mo}}^4 + \gamma_{\text{a}}^4)^{1/4}},$$
 (8)

which is equivalent to $b_{21,\text{shft}} \approx 2\delta_{\text{mo}}[Y(1-T_{\text{F}})]^{1/4}$ in terms of the forward transmission from port 1 to port 2 (a factor of $[Y(1-T_{\text{F}})]^{-1/4}$ higher than the equivalent single ring circulator).

The same system can be operated in EP mode by using contra-directional MO shifts such that the positive MO-shifted resonance frequency of CW light in the lower ring is equal to the negative MO-shifted resonance frequency of CCW light in the upper ring. That is, the rings are initially detuned in the absence of a magnetic field such that the MO shifts push them into resonance when light is incident from port 2 (corresponding to the EP condition, $\delta_1 = \delta_2$) and farther out of resonance when light is incident from port 1 ($\delta_1 \rightarrow \delta_1 - \delta_{mo}$ and $\delta_2 \rightarrow \delta_2 + \delta_{mo}$). This breaks the EP, yielding the central transmission maximum in $|S_{21}|^2$ and corresponding minimum in $|S_{31}|^2$ shown in Fig. 3(b) and Fig. 3(c), respectively. The isolation bandwidth between ports 1 and 2 in this case is:

$$b_{21,\text{ep}} = \frac{2\sqrt{\delta_{\text{mo}}}\gamma_{\text{a}}Y^{1/4}(\delta_{\text{mo}}^2 + \gamma_{\text{a}}^2)^{1/4}}{(2\delta_{\text{mo}}^2 + \gamma_{\text{a}}^2)^{1/2}},\tag{9}$$

which exhibits the characteristic $\sqrt{\delta_{\rm mo}}$ dependence of EP operation when $\delta_{\rm mo}$ is small compared to the coupling/loss rates in the system. Figure 3(d) shows that, in addition to maintaining a larger isolation bandwidth as $\delta_{\rm mo}$ grows small, the forward transmission loss for EP operation is also reduced relative to shift operation. Figure 3(e) summarizes both effects, demonstrating that, for the same MO frequency split, insertion loss, and isolation ratio, EP operation enables a higher isolation bandwidth. The increase can be estimated analytically by rewriting Eq. 9 as $b_{21,\rm ep} \approx 2b_{21,\rm shft}[(1-T_{\rm F})(4-3T_{\rm F})/T_{\rm F}(4-2T_{\rm F})^2]^{1/4}$, which amounts to $\sim 1.5\times$ at 3 dB insertion loss.

The advantage of EP operation is less significant between ports 1 and 3 as shown in Fig. 3(f) because high extinction in $|S_{31}|^2$ requires high transmission in $|S_{21}|^2$ by conservation of energy, which is the low insertion loss/large δ_{mo} regime where the EP effect diminishes in Fig. 3(d). We note that, in principle, the EP-critical coupling condition, $\gamma_a - \gamma_1 = \gamma_b + \gamma_2 = \kappa$, implies that the circulator (the circulation path is port $1 \to 2 \to 4 \to 3 \to 1$) can only function symmetrically (i.e. the same for light incident at any input port) when dissipation in the rings is negligible,

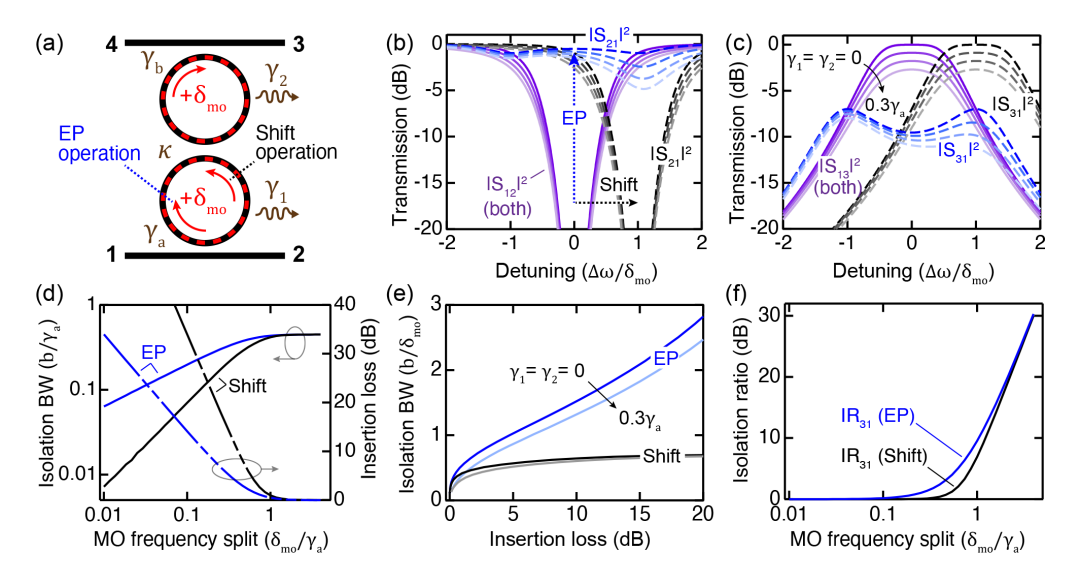


Fig. 3. (a) Schematic of a coupled ring circulator where light propagating from one port to another experiences either the same (shift operation) or opposite (EP operation) MO resonance frequency shifts in each ring. Non-reciprocal transmission spectra are shown for each mode of operation between ports 1 and 2 in (b) and ports 1 and 3 in (c). In these plots, $\gamma_a = \gamma_b = \kappa = \delta_{mo}$ and each family of curves shows the effect of increasing dissipation ($\gamma_1 = \gamma_2$) in each ring. (d) Different scaling of isolation bandwidth (20 dB) and insertion loss between ports 1 and 2 for the EP and shift modes of operation. These curves are for the ideal case of lossless rings; they change negligibly when loss is included as summarized in (e). (f) The isolation ratio between ports 1 and 3 is similar for the two modes of operation.

 $\gamma_{1,2} \ll \gamma_{a,b}$. It turns out, however, that this is not a strict condition and the benefits of EP operation remain robust even when loss is non-negligible, as evident from the lighter colored lines in Fig. 3(b)-(e).

To validate the temporal coupled mode theory treatment above, we use Lumerical [26] to simulate the circulator from Fig. 3(a) assuming the same geometry and material parameters as in Ref. [11], except with a smaller ring radius of 10 µm that minimizes the combined material and bending loss. Figure 4(a) shows the MO splitting in modal effective indices ($n_{\text{eff},\pm}$) for each ring as well as the ring-to-ring and ring-to-guide power coupling coefficients (K_{rr} and K_{rg} , respectively), which target the critical coupling condition, $K_{\text{rr}} = K_{\text{rg}}^2/(2 - K_{\text{rg}})^2$, at $\lambda = 1550$ nm [24]. These results are then used with the transfer matrix method [24] to calculate the transmission spectra plotted in Fig. 4(b), with equal ring radii for shift operation and slightly different radii, $R_1/R_2 = n_{\text{eff},+}/n_{\text{eff},-}$, for EP operation (the rings would be thermally tuned in practice) since the NRPS brings the rings into resonance for light propagating in one direction and pushes them further out of resonance for light propagating in the other direction.

Associating the parameters in Fig. 4(a) with their temporal coupled mode theory counterparts, we find good agreement between the two modeling approaches in Fig. 4(b), as well as with the prior results of Ref. [11]. The EP mode splitting is obvious in the cross port spectra ($|S_{31}|^2$) of Fig. 4(b) but is less clear in the thru port case ($|S_{21}|^2$) because the ~ 37 dB cm⁻¹ modal propagation loss in the rings (due mainly to absorption in the Ce:YIG layer) causes the lower wavelength minimum to dominate.

Figure 4(c) shows the average isolation bandwidth (20 dB) [21] for the thru port as a function of the average (over the same bandwidth) insertion loss, which is varied by changing the coupling gap widths to adjust K_{rr} and K_{rg} . As in Fig. 3(e), the advantage of operating in EP mode grows as

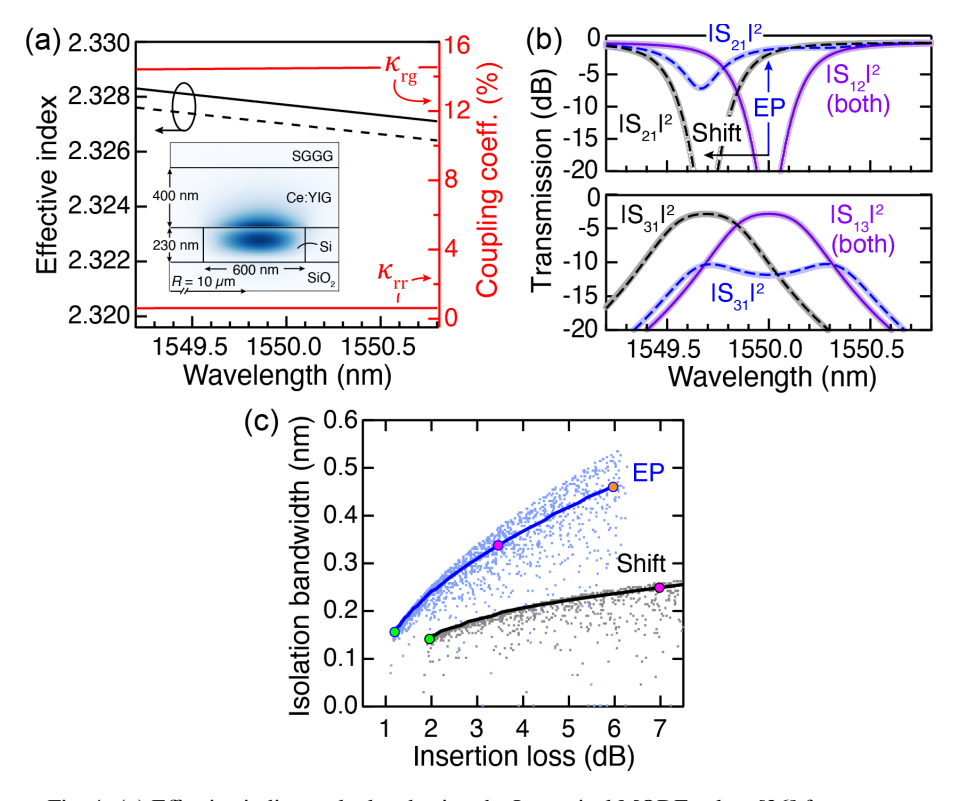


Fig. 4. (a) Effective indices calculated using the Lumerical MODE solver [26] for counterpropagating modes in the MO rings of Fig. 3(a) assuming a ring radius of 10 µm and the waveguide structure shown in the inset; details of the structure are provided in Ref. [11]. The ring-to-ring (K_{rg}) and ring-to-bus waveguide (K_{rr}) power coupling coefficients simulated using the Lumerical FDTD solver [26] are shown on the right-hand scale for gap thicknesses of 150 nm and 400 nm, respectively. The optical constants of each material are the same as in Ref. [11] except for a smaller Faraday rotation of -2000°cm⁻¹ in the cerium-substituted yttrium iron garnet (Ce:YIG) layer [27]. The imaginary component of the effective index (not shown) corresponds to a modal propagation loss of $\sim 37~\mathrm{dB\,cm^{-1}}$. (b) Non-reciprocal thru and cross port transmission spectra computed for shift and EP mode operation based on the parameters in (a) using the transfer matrix method (dark lines) and temporal coupled mode theory (faint background lines) for comparison; the rates in the latter case are $\gamma_a = \gamma_b = \kappa = 34.5$ GHz, $\gamma_1 = \gamma_2 = 11.5$ GHz, and $\delta_{mo} = 39$ GHz. (c) 20 dB isolation bandwidth between ports 1 and 2 as a function of the insertion loss obtained by varying the ring-to-ring (d_{rr}) and ring-to-guide (d_{rg}) gap thicknesses. The solid lines show the case where the gaps satisfy the critical coupling condition and the scattered dots show the result of normally-distributed random deviations in the gap thicknesses with a standard deviation, $\sigma = 2$ nm [28]. The filled green circles on each curve correspond to the spectra in (b) with gap thicknesses (d_{rg} , d_{rr})=(150, 400) nm; magenta, and orange circles correspond to gap thicknesses of (97, 280) nm and (60, 188) nm, respectively.

the coupling coefficients are increased (by decreasing the corresponding gap widths), broadening the modal linewidths relative to the $\Delta\lambda\sim0.3$ nm resonant wavelength split. To this point, operating a typical circulator in EP instead of shift mode cuts its insertion loss by roughly a factor of two while boosting its isolation bandwidth by $\sim50\%$, as exemplified by the magenta markers on each line.

Notably, this performance enhancement does not come at the expense of reduced fabrication tolerance, as the scatter that results from likely coupling gap variations [28] in the Monte Carlo analysis of Fig. 4(c) is similar for EP and shift mode operation. In fact, many of the random realizations in the EP case yield a larger isolation bandwidth than the nominal critical coupling condition (solid line). This happens when the rings are slightly overcoupled (realizations where the ring-to-ring gap is narrower than nominal) and the extinction minimum of the backward transmission spectrum begins to split, thereby broadening the bandwidth. This split is detrimental to shift mode operation and thus all of its realizations lie below the critical coupling line. One final practical benefit of EP operation is that it can be implemented for transverse electric (TE) mode isolation by applying a uniform magnetic field normal to the plane of the rings, whereas the field has to invert its direction between the rings for shift mode operation.

Moving forward, it seems likely that systems with higher order EPs [17] (constructed using, e.g. the hierarchical method of Ref. [29]) could further improve the isolation bandwidth-insertion loss tradeoff, though the value of doing this would ultimately depend on whether it justifies the added complexity. More generally, the fact that loss is required for EPs to exist in the first place may lead it to be viewed as a resource, for example by incentivizing operation closer to optical transitions where the MO response is resonantly enhanced [27]. The opportunity is evident even for the single ring case, where operating with the same MO figure of merit [30] (i.e. the ratio of Verdet constant to absorption coefficient, which is proportional to $\delta_{\rm mo}/\gamma_0$ in the formalism here) near a lossy transition, as opposed to far from one, increases the isolation bandwidth per Eq. 3 without affecting the insertion loss since the latter is independent of $\delta_{\rm mo}/\gamma_0$. In this context, we note that our analysis neglects nonreciprocal loss (the Kramers-Kronig counterpart of NRPS) for simplicity; it can be included by taking $\delta_{\rm mo}$ to be complex, though the effect tends to be minor.

3. Conclusion

In summary, we have shown that operating ring isolators at an EP causes their isolation bandwidth to depend sublinearly on NRPS, which enhances the performance that can be achieved from the weak MO response of current materials. The essence of this result can be recast in plain language simply by saying that it is more effective to use a given NRPS to split a coupled ring resonance than to shift one.

Although the treatment here is focused on MO isolators, other weak nonreciprocal perturbations [2, 3] could presumably also leverage an appropriately-constructed EP to improve isolator performance. Beyond passive isolators, the bigger opportunity may actually lie in active systems (e.g. with gain in the top ring of Fig. 1(a,ii) and MO response in the bottom ring) given the overarching desire to integrate lasers and isolators in most photonic integrated circuit applications. While the basic threshold behavior of EP lasers is already worked out in Refs. [22, 31–33], the extent to which an above-threshold MO device is immune to its own reflected light (i.e. avoiding dynamical and phase instabilities) is not yet clear and should provide fertile ground for future study.

Funding

This work was supported by DARPA Award no. N66001-20-1-4052.

Disclosures

The authors declare no conflicts of interest.

Data availability statement

The data that support the findings of this study are available from the corresponding author upon reasonable request.

References

- Y. Shoji, K. Miura, and T. Mizumoto, "Optical nonreciprocal devices based on magneto-optical phase shift in silicon photonics," J. Opt. 18, 013001 (2015).
- H. Lira, Z. Yu, S. Fan, and M. Lipson, "Electrically driven nonreciprocity induced by interband photonic transition on a silicon chip," *Phys. Rev. Lett.* 109, 033901 (2012).
- 3. E. A. Kittlaus, W. M. Jones, P. T. Rakich, N. T. Otterstrom, R. E. Muller, and M. Rais-Zadeh, "Electrically driven acousto-optics and broadband non-reciprocity in silicon photonics," *Nat. Photonics* 15, 43–52 (2021).
- Y. Shi, Z. Yu, and S. Fan, "Limitations of nonlinear optical isolators due to dynamic reciprocity," Nat Photon 9, 388–392 (2015).
- L. Bi, J. Hu, P. Jiang, D. H. Kim, G. F. Dionne, L. C. Kimerling, and C. A. Ross, "On-chip optical isolation in monolithically integrated non-reciprocal optical resonators," *Nat. Photonics* 5, 758–762 (2011).
- N. Kono, K. Kakihara, K. Saitoh, and M. Koshiba, "Nonreciprocal microresonators for the miniaturization of optical waveguide isolators," Opt. Express 15, 7737 (2007).
- P. Pintus, F. Di Pasquale, and J. E. Bowers, "Design of transverse electric ring isolators for ultra-low-loss Si_3n_4 waveguides based on the finite element method," Opt. Lett. 36, 4599 (2011).
- M.-C. Tien, T. Mizumoto, P. Pintus, H. Kromer, and J. E. Bowers, "Silicon ring isolators with bonded nonreciprocal magneto-optic garnets," Opt. Express 19, 11740 (2011).
- 9. D. Huang, P. Pintus, C. Zhang, Y. Shoji, T. Mizumoto, and J. E. Bowers, "Electrically driven and thermally tunable integrated optical isolators for silicon photonics," *IEEE J. Sel. Top. Quantum Electron.* 22, 271–278 (2016).
- W. Qi, Y. Jin, H. Yu, and X. Jiang, "A magneto-optical isolator based on series-coupled race-track resonators," *Jpn. J. Appl. Phys.* 54, 012601 (2015).
- P. Pintus, D. Huang, C. Zhang, Y. Shoji, T. Mizumoto, and J. E. Bowers, "Microring-Based Optical Isolator and Circulator with Integrated Electromagnet for Silicon Photonics," *J. Light. Technol.* 35, 1429–1437 (2017).
- Y. Shoji, T. Mizumoto, H. Yokoi, I. W. Hsieh, and R. M. Osgood, "Magneto-optical isolator with silicon waveguides fabricated by direct bonding," Appl. Phys. Lett. 92, 071117 (2008).
- 13. Q. Du, C. Wang, Y. Zhang, Y. Zhang, T. Fakhrul, W. Zhang, C. Gonçalves, C. Blanco, K. Richardson, L. Deng, C. A. Ross, L. Bi, and J. Hu, "Monolithic On-chip Magneto-optical Isolator with 3 dB Insertion Loss and 40 dB Isolation Ratio," ACS Photonics 5, 5010–5016 (2018).
- 14. Y. Zhang, Q. Du, C. Wang, T. Fakhrul, S. Liu, L. Deng, D. Huang, P. Pintus, J. Bowers, C. A. Ross, J. Hu, and L. Bi, "Monolithic integration of broadband optical isolators for polarization-diverse silicon photonics," *Optica* 6, 473 (2019).
- 15. W. Yan, Y. Yang, S. Liu, Y. Zhang, S. Xia, T. Kang, W. Yang, J. Qin, L. Deng, and L. Bi, "Waveguide-integrated high-performance magneto-optical isolators and circulators on silicon nitride platforms," *Optica* 7, 1555 (2020).
- 16. M.-A. Miri and A. Alù, "Exceptional points in optics and photonics," Science 363, eaar7709 (2019).
- 17. H. Hodaei, A. U. Hassan, S. Wittek, H. Garcia-Gracia, R. El-Ganainy, D. N. Christodoulides, and M. Khajavikhan, "Enhanced sensitivity at higher-order exceptional points," *Nature* **548**, 187–191 (2017).
- 18. J. Wiersig, "Review of exceptional point-based sensors," Photonics Res. 8, 1457 (2020).
- 19. H. A. Haus, Waves and fields in optoelectronics (Prentice-Hall,, 1984).
- H. A. Haus and W. Huang, "Coupled-mode theory," Proc. IEEE 79, 1505–1518 (1991). Conference Name: Proceedings of the IEEE.
- D. Huang, "Integrated Optical Isolators and Circulators for Heterogeneous Silicon Photonics," Ph.D. thesis, University of California, Santa Barbara, Santa Barbara, CA, USA (2019).
- D. D. Smith, H. Chang, L. Horstman, and J.-C. Diels, "Parity-time-symmetry-breaking gyroscopes: lasing without gain and subthreshold regimes," Opt. Express 27, 34169 (2019).
- 23. W. Bogaerts, P. de Heyn, T. van Vaerenbergh, K. de Vos, S. Kumar Selvaraja, T. Claes, P. Dumon, P. Bienstman, D. van Thourhout, and R. Baets, "Silicon microring resonators," *Laser Photonics Rev.* 6, 47–73 (2012).
- C. L. Manganelli, P. Pintus, F. Gambini, D. Fowler, M. Fournier, S. Faralli, C. Kopp, and C. J. Oton, "Large-FSR Thermally Tunable Double-Ring Filters for WDM Applications in Silicon Photonics," *IEEE Photonics J.* 9, 6600310 (2017).
- M. J. Grant and M. J. F. Digonnet, "Enhanced rotation sensing and exceptional points in a parity-time-symmetric coupled-ring gyroscope," Opt. Lett. 45, 6538-6541 (2020).
- 26. Ansys/Lumerical, https://www.lumerical.com/ansys/.

- M. C. Onbasli, L. Beran, M. Zahradník, M. Kucera, R. Antoš, J. Mistrík, G. F. Dionne, M. Veis, and C. A. Ross, "Optical and magneto-optical behavior of Cerium Yttrium Iron Garnet thin films at wavelengths of 200-1770 nm," Sci. Reports 6, 1–10 (2016).
- Z. Lu, J. Jhoja, J. Klein, X. Wang, A. Liu, J. Flueckiger, J. Pond, and L. Chrostowski, "Performance prediction for silicon photonics integrated circuits with layout-dependent correlated manufacturing variability," *Opt. Express* 25, 9712–9733 (2017).
- Q. Zhong, J. Kou, S. K. Ozdemir, and R. El-Ganainy, "Hierarchical Construction of Higher-Order Exceptional Points," Phys. Rev. Lett. 125, 203602 (2020).
- 30. A. R. Taussig, G. F. Dionne, and C. A. Ross, "Dependence of Faraday rotation and magneto-optical figure of merit on dielectric tensor elements in materials with uniaxial symmetry," *Phys. Rev. B Condens. Matter Mater. Phys.* 77, 012407 (2008).
- H. Hodaei, M. A. Miri, A. U. Hassan, W. E. Hayenga, M. Heinrich, D. N. Christodoulides, and M. Khajavikhan, "Parity-time-symmetric coupled microring lasers operating around an exceptional point," *Opt. Lett.* 40, 4955–4958 (2015).
- 32. A. U. Hassan, H. Hodaei, M.-A. Miri, M. Khajavikhan, and D. N. Christodoulides, "Nonlinear reversal of the PT-symmetric phase transition in a system of coupled semiconductor microring resonators," Phys. Rev. A 92, 063807 (2015).
- 33. H. Hodaei, M.-A. Miri, M. Heinrich, D. N. Christodoulides, and M. Khajavikhan, "Parity-time–symmetric microring lasers," *Science* **346**, 975–978 (2014).